EDGE ARTICLE

Check for updates

Union carbide polymerization catalysts: from uncovering active site structures to designing molecularly-defined analogs†

David Trummer,‡ Anna Giorgia Nobile,‡ Pierre-Adrien Payard, [ID] ‡ Anton Ashuiev, Yuya Kakiuchi, Daniel Klose, [ID] Gunnar Jeschke* and Christophe Copéret [ID] *

The Union Carbide (UC) ethylene polymerization catalysts, based on chromocene dispersed on silica, show distinct features from the Phillips catalysts, but share the same heated debate regarding the structure of their active sites. Based on a combination of IR, EPR spectroscopies, labeling experiments, and DFT modeling, we identified monomeric surface-supported Cr(III) hydrides, $(\equiv SiO)Cr(Cp)-H$, as the active sites of the UC catalyst. These sites are formed in the presence of grafted and adsorbed chromocene as well as residual surface OH groups, only possible at high Cr loading, and involve a C–H activation of the Cp ring. These Cr-hydrides initiate polymerization, yielding Cr(III) alkyl species that insert ethylene through a Cossee–Arlman-type mechanism, as evidenced by spectroscopic studies. These insights inspired the design of a well-defined analog, $CpCr(CH(SiMe_3)_2)_2$ grafted on partially dehydroxylated silica, that shows similar spectroscopic and polymer structure to the UC catalyst, further supporting the proposed active site structure.

1 Introduction

Polyethylene (PE) is one of the most commonly used plastics worldwide.[1] Since the 1950s, its production mostly relies on Ziegler–Natta or Phillips catalysts.[1] In the early 1970s, an alternative Cr-based Union Carbide (UC) catalyst was developed based on silica-supported chromocene, $[Cp_2Cr(II)]$ (**1**).[2–4] The UC catalyst is probably one of the first industrially used heterogeneous catalysts prepared from a silica supported organometallic reagent, thus pioneering the field of surface organometallic chemistry (SOMC).[5,6] This catalyst shows high activity towards ethylene polymerization (EP) and its high response to H_2 allows for chain length control.[4,7–10]

Despite years of research and its unique features, its active sites and operating mechanism are unknown and still debated (Fig. 1A). The diversity of surface species, together with the low number of active sites (few %), have made the elucidation of the active site and mechanism challenging.[9] Notably, the density of hydroxyl groups on the silica support influences the activity, which increases with decreasing OH density.[11] A variety of Cr sites were previously reported: based on IR and UV-vis

investigations, both mono-grafted **1**, *i.e.* $(\equiv SiO)CrCp$ and chemisorbed **1** (*i.e.* $Cp_2Cr\cdots SiO_2$) at higher Cr loadings (Fig. 1A) were detected.[4,7,12] The former was suggested to generate the corresponding monomeric Cr(IV) metallacycle (Fig. 1A, right) in the presence of ethylene.[13] X-ray absorption spectroscopic (XAS) studies provided evidence for dimeric silica-supported Cr(III) species $Cp_2Cr_2O_4$ before ethylene treatment.[14] Dimeric half-sandwich Cr(II) sites on silica have also been identified, based on ^1H MAS NMR investigations.[8] The latter were proposed to react with C_2H_4 to yield dimeric Cr(III) alkyl silicates (Fig. 1A, right).[13]

In parallel, Theopold developed model systems based on molecular cyclopentadienyl Cr complexes, and showed that well-defined Cr(III) alkyls are able to insert ethylene, suggesting that the active sites of the UC catalyst could have similar electronic structure.[15]

In this work (Fig. 1B), we selectively prepare and characterize the Cr surface sites of the UC catalyst, using SOMC combined with spectroscopic and computational studies. In Part 1, using CO as a probe molecule for IR investigations, we identify various surface Cr sites as a function of Cr loadings and support our assignments by comparison with well-defined model systems prepared *via* SOMC. We evidence the presence of surface Cr hydrides in the UC catalysts at high loading, whose presence is confirmed by EPR spectroscopy. In Part 2, we investigate possible pathways for Cr–H formation using ^2H labeling and DFT calculations. The CO vibrational frequencies of the proposed sites are calculated at the DFT level and compared with the experimental ones to validate the previously described
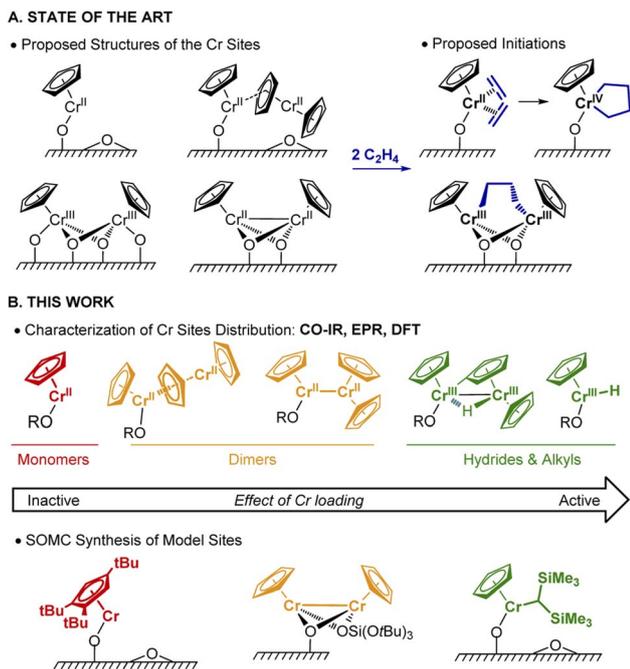
Fig. 1 (A) Previously proposed surface site structures of the UC catalyst. (B) Illustration of Cr sites (above the arrow) investigated by CO-IR, EPR, and DFT modeling as a function of the Cr loading. The respective well-defined monomeric, dimeric Cr(II), and monomeric alkyl-Cr(III) sites, (below the arrow) are prepared *via* SOMC.

assignments. Overall, we propose that two Cr moieties are cooperating to generate supported monomeric and dimeric Cr(III) hydrides *via* C–H activation of the Cp ring. In Part 3, using DFT calculations, we show that monomeric Cr(III) hydrides initiate EP *via* C_2H_4 insertion into the Cr(III)–H bond with the subsequent formation of Cr(III) alkyl species, enabling further polymerization. Finally, in Part 4, we develop a molecularly-defined analog of the proposed active site – namely ($\equiv$SiO) CrCp[CH(SiMe$_3$)$_2$]. This Cr(III)-alkyl initiates EP, as evidenced by EPR hyperfine spectroscopy and generates a similar polymer, further supporting that the active sites of the UC catalysts correspond to surface CpCr(III) hydrides/alkyls.

2 Results and discussion

2.1. Characterization of monomeric Cr(III)–H by CO-IR probe and EPR spectroscopies

While solving the structure of the active site of the UC catalyst is challenging, its identification should be possible, providing one detects a spectroscopic signature that correlates with polymerization activity.[10] As reported earlier,[2–4] the EP activity of the UC catalyst is critically dependent on the Cr loading. We therefore prepared and investigated four different catalysts varying in Cr loadings: **1-SiO$_2$-0.25, 1-SiO$_2$-0.5, 1-SiO$_2$-1,** and **1-SiO$_2$-2** that contain 0.25, 0.5, 1.0, and 2.0 wt% of Cr, respectively (ESI, Section S2.1† for preparation). Contacting **1** with partially dehydroxylated silica at 700 °C (SiO$_{2-700}$)[6] led to a color change of the material, from white to dark blue/black and a decrease of the IR bands corresponding to the surface OH groups (Fig. S1).†

According to elemental analysis and ^{1}H NMR quantifications of the washing solutions (Section S2.1 and Table S1),† about one Cp/Cr is present on silica for **1-SiO$_2$-0.25**, suggesting the presence of mainly mono-grafted sites. The Cp/Cr ratio increases with increasing Cr loading, reaching almost 3 Cp/2 Cr in **1-SiO$_2$-1**, suggesting the presence of both grafted and strongly adsorbed **1** on silica. The EP activities for all the obtained materials show the following trends: while **1-SiO$_2$-1** and **1-SiO$_2$-2** are EP active, the low loading materials **1-SiO$_2$-0.25** and **1-SiO$_2$-0.5** show hardly any activity (Table S2).† Therefore, high Cr loadings (>1.0 wt% of Cr) favors the generation of the active sites in UC catalysts, consistent with previous findings.[4]

IR spectroscopy using CO as a probe molecule[6] was used to characterize the prepared UC catalysts (Fig. 2) and identify possible Cr surface sites (Section S1).† We assigned the various IR bands by comparison with the ones obtained for well-defined Cr surface species prepared by SOMC (Fig. 1B and 2, **2-SiO$_2$** and **3-SiO$_2$**).

The low-loading material **1-SiO$_2$-0.25** after exposition to CO shows only two predominant CO bands at 2061 cm^{-1} and 1981 cm^{-1} (Fig. 2A, red region). These bands disappear upon
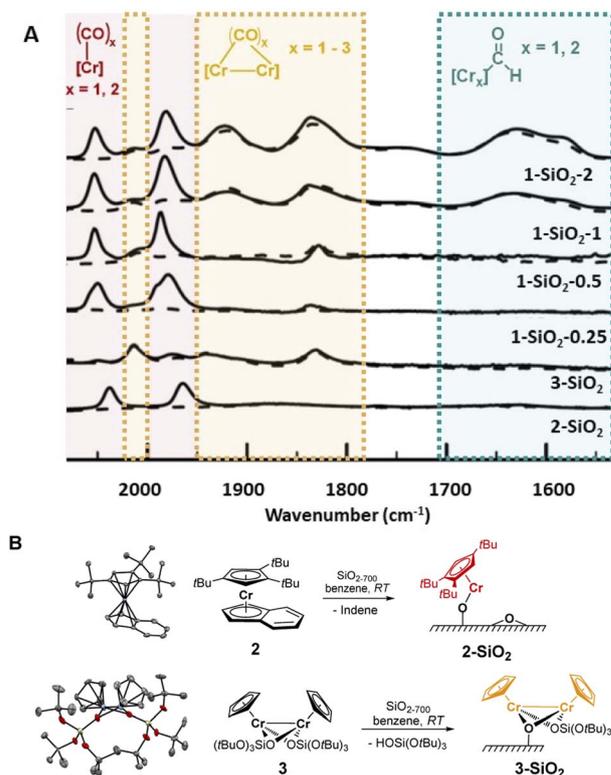

Fig. 2 (A) Background-subtracted IR spectra (solid lines) of the UC catalysts with different Cr loadings and model systems **2-SiO$_2$** and **3-SiO$_2$** (Fig. 2B) after exposure to CO (25 mbar). Dashed lines indicate the IR spectra after the exposure to high vacuum (10^{-5} mbar). Reversible CO bands are marked in red (indicative of monomeric Cr(II) sites). Bands from irreversibly bound CO molecules are marked in orange (indicative of bridging CO between interacting Cr atoms). Low energy CO bands are marked in green (indicative of formyl groups). (B) Grafting of tailored monomeric and dimeric model complexes on SiO$_{2-700}$.

high vacuum (10^{-5} mbar; Fig. 2A, dashed lines), indicating the reversible and weak CO binding to these Cr surface sites. While increasing the Cr loading to 0.5 wt% (**1-SiO$_2$-0.5**), three additional bands at 2015 cm^{-1}, ~1905 cm^{-1} (broad) and 1837 cm^{-1} arise (Fig. 2A, orange region). In contrast to the previously observed bands (Fig. 2A, red region), these bands are formed irreversibly, indicating a stronger CO binding to the Cr sites. Upon further increasing the Cr content to 1 wt% (**1-SiO$_2$-1**), three additional broad CO bands appear at 1742 cm^{-1}, 1630 cm^{-1}, and 1579 cm^{-1} (Fig. 2A, green region).[16] Notably, the appearance of the latter signals correlates with EP activity.

We then focused on the assignment of the CO-IR bands observed in the three groups (red, orange, green). The two reversible bands, together with a small shoulder at 1993 cm^{-1} (Fig. 2A, red) may be assigned to monomeric Cr surface sites. Indeed, the well-defined silica-supported monomeric Cr(II) [($\equiv$SiO)Cr(*tttt*Cp)] **2-SiO$_2$** (Fig. 2B, Section S2.2, and Fig. S3 for the IR spectra, S4† for XANES analysis) shows two reversible bands at 2035 cm^{-1} and 1960 cm^{-1} upon exposition to CO (Fig. 2A), as observed for **1-SiO$_2$-0.25**. Therefore, the two signals in the red region are assigned to the symmetric and antisymmetric CO stretching modes of di-carbonylic, monomeric Cr(II) sites.[17] Notably, the well-defined Cr(II) monomeric species in **2-SiO$_2$** show no EP activity at 10 bars and 40 °C, indicating that monomeric Cr(II) sites are not able to polymerize ethylene.

For **1-SiO$_2$-0.5** (Fig. 2A, orange region), the irreversibility of CO adsorption could arise due to bridging CO molecules between two Cr centers, suggesting the presence of dimeric Cr surface sites. The well-defined dimeric Cr(II) surface site **3-SiO$_2$** (Fig. 2B, ESI Section S2.3 & Fig. S6–S9†) shows four bands between 2012 cm^{-1} and 1830 cm^{-1} resulting from irreversibly bound CO molecules. These IR frequencies are consistent with the CO bands observed in **1-SiO$_2$-0.5** (Fig. 2A, orange region). Therefore, we attribute these IR bands to the dimeric Cr(II) sites of the UC catalyst. Similar to **2-SiO$_2$**, **3-SiO$_2$** shows no EP activity, indicating that the active sites of the UC catalyst do not correspond to monomeric or dimeric Cr(II) species.

This encouraged us to further investigate the surface species associated with the low energy CO bands (Fig. 2A, green region), which become significant only for the **1-SiO$_2$-1** and **1-SiO$_2$-2** materials (Fig. S10–11).† The CO vibrational frequencies down to 1550 cm^{-1} suggest the presence of formyl groups bound to Cr,[18] that could result from the CO insertion into a Cr–H bond. While similar complexes, [Cp*CrPR$_3$(CO)$_2$CHO],[18] have been formed upon the reaction of [Cp*Cr(PR$_3$)(CO)$_3$] with a hydride source, the formation of formyl intermediates *via* migratory insertion of CO is rare for early transition metals, but has been documented with zirconium hydride, a textbook example.[19] Therefore, we propose that the UC catalysts with higher Cr loading are likely associated with the formation of surface-supported Cr hydrides. Since the IR bands of formyl grow in intensity for the UC catalysts active in EP (Fig. 2A), the proposed Cr–H could be the active or initiating sites, in analogy with previously described C$_2$H$_4$ polymerizing Ti hydrides.[20]

To inquire the possible presence of surface Cr hydrides as initiation sites of EP, we carried out 2D J-mediated heteronuclear multi-quantum correlation (HMQC)[20] MAS NMR of **1-SiO$_2$-1** after exposure to ^{13}C$_2$D$_4$. The HMQC spectrum (Fig. S12B†) shows narrow and well-resolved correlations between the ^{13}C signals at 29 and 31 ppm and the ^{1}H signal at 1.5 ppm, indicating the presence of ^{1}H in the obtained PE.[21–23] The proton source has to originate from the surface OH groups or the Cp ligands. IR investigations of the same experiment show a weak band (Fig. S12A,† shown in green) at 2887 cm^{-1} related to a –CH stretching and an additional –CD$_2$-stretching. This signals imply the presence of C–H vibrations, which could be assigned to the end –CD$_2$H group resulting from multiple insertions of C$_2$D$_4$ into Cr hydrides as initiating sites.[24,25] All together, these results support a hydride-mediated initiation mechanism.

The potential activity of Cr–H raises questions about the Cr oxidation state of these species. Previous work suggests the presence of Cr(III) sites in the UC system,[14] we therefore performed EPR studies of the catalysts. We found that the CW EPR spectrum of **1-SiO$_2$-1** (Cp$_2$Cr^{II} on silica) contains paramagnetic species, even before contacting with C$_2$H$_4$ (Fig. S13A,† top), which are consistent with Cr(III) surface sites. The major fraction is represented by a nearly axial monomeric low-spin Cr(III) species. It appears that the EPR signature of this species changes upon contact with C$_2$H$_4$ (Fig. S13B†); the *g* tensor of this newly formed species is better fitted as being orthorhombic (Fig. S13A,† bottom) with an increased g_x value, consistent with a change in the ligand surrounding of the LS Cr(III) sites after the contact with C$_2$H$_4$. This finding suggests that the observed Cr(III) species are the active sites of EP and likely a surface Cr hydride, as discussed above.

To summarize, while both mono- and dimeric Cr(II) surface sites are identified in the UC system, they are not active in EP. At higher Cr loadings, surface-supported Cr(III) hydride species are also formed; their presence correlates with EP activity and are thus likely associated with the active site of the UC catalyst.

2.2. Formation and characterization of surface Cr hydrides

In the next step, we investigated the possible pathways for the formation of these Cr(III) hydrides. In molecular systems, the formation of binuclear bridging Cr hydride complexes was previously reported,[26–29] and in analogy to Cr, dinuclear bridging molybdocene–hydride complexes with activated Cp ligands are also known.[30] Monomeric Cr hydrides are scarce,[31] however, Sinema *et al.* reported a C–H activation step at the Cp ligand on ansa–chromocene complexes in the presence of [H(OEt$_2$)$_2$BAr$_4$],[32] and related activation pathways were also reported for other 3d metallocene-based complexes.[33,34]

To elucidate whether the related C–H activation of the Cp ligand could take place on the surface, we grafted perdeuterated chromocene (**1$_{d10}$**) on silica. If the C–D activation on the Cp ring is possible, D might exchange with surface OH groups, resulting in the appearance of an IR band corresponding to Si–OD groups. This IR band is indeed observed and suggests that C–H activation at the Cp ring is feasible (Fig. 3).

To elucidate how the C–H activation can take place, we performed subsequent grafting of non-labeled (**1**) and perdeuterated (**1$_{d10}$**) chromocene and *vice versa* (Section S2.4 and

$(C_5D_5)_2Cr + SiOH \rightleftharpoons (C_5D_{5-x}H_x)_2Cr + x\ SiOD$
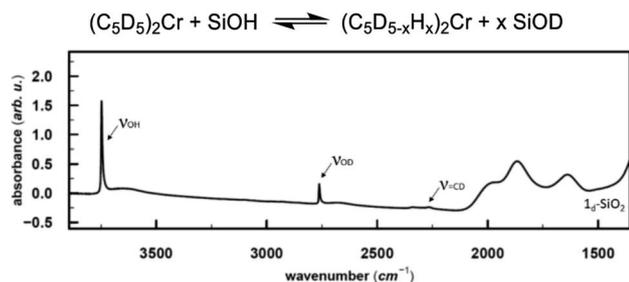

Fig. 3 Top: Proposed reaction for the interaction of 1_{d10} with surface OH groups, resulting in D exchange of deuterated Cp rings. Bottom: IR spectrum of D-labeled $1\text{-SiO}_2\text{-}1$. In addition to the =CD band, consistent with the deuterated Cp ring, the Si–OD band arises from the H/D exchange with the silica surface.

Fig. S14†). When $1_{ll\text{-}d}\text{-SiO}_2\text{-}1$ (0.25 wt% 1_{d10} & 0.75 wt% **1**) is exposed to C_2H_4, only trace amounts of –CH_2D end groups are observed in the IR spectrum (Fig. S15),† while after polymerization of C_2D_4, mainly –CD_2H end groups are observed. This suggests that the C–H activation takes place on the chemisorbed **1** (see Fig. S15).† Congruent results are obtained when exposing $1_{hl\text{-}d}\text{-SiO}_2\text{-}1$ (0.25 wt% **1** & 0.75 wt% 1_{d10}) to labeled and non-labeled ethylene (Fig. S15†).[35]

We performed DFT studies to explore possible reaction pathways of the reaction of **1** with the silica surface (modeled by $RO = -Si(OH)_3$). This simple model cannot account for secondary interactions with the surface, thus the computed pathways for the formation of the Cr-hydride species (Fig. 4) should be considered as providing a qualitative insight on the feasibility of the C–H activation process, but cannot be used to
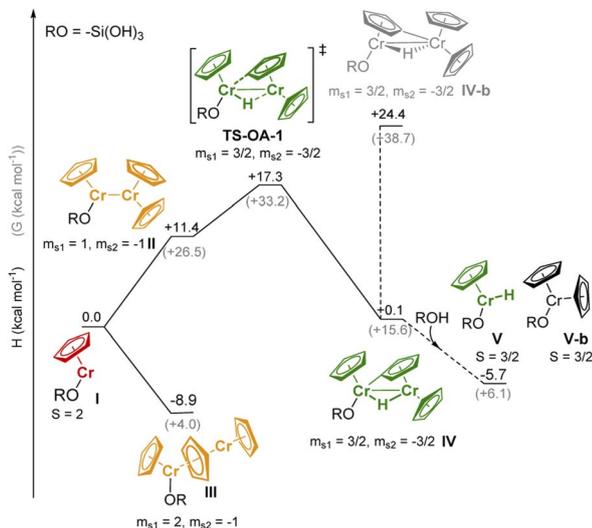

Fig. 4 Proposed reaction pathways for the interaction of **1** on partially dehydroxylated silica. Enthalpies (H kcal mol^{-1}) and free energies (G kcal mol^{-1}) are calculated with respect to **I** and $CrCp_2$. For monomeric sites, the spin quantum number is indicated with S; for dimeric sites, the local projection of the spin, as obtained from the Mulliken spin density on [CrCp] fragments I, is shown with m_{si}. Since the formation of dimers is artificially disfavored given the approximations on the estimation of the entropy, only the enthalpy will be discussed in the text.

assess the relative stability of surface species. The structures of the Cr species (Tables S5 and S6† for the DFT-optimized structures) were optimized using unrestricted open-shell calculations with the B3LYP functional (see ESI and Table S4† for the computational details and optimization of the computational method) and the spin state with the lowest energy was selected (Table S7†). Dimeric species were modeled using the broken symmetry approach.[36]

The high-spin ($S = 2$) mono-grafted site **I** (see Fig. 4 and Table S7),† is coordinatively unsaturated and may interact with adjacent Si–O–Si bridges or surface OH groups. At higher Cr loading, site **I** can also interact with another molecule of **1**, either to form stacked metallocene complex **III** ($\Delta H = -8.9$ kcal mol^{-1}), or complex **II** with a direct Cr–Cr bond (site **II**, $\Delta H = +11.4$ kcal mol^{-1}). Sites **II** can further reorganize through C–H activation at the Cp ring, yielding the surface site **IV**, a bridging Cr(III)–hydride complex (**TS-OA-1**, $\Delta H^{\ddagger} = +17.3$ kcal mol^{-1}). The C–H activation at the other Cr moiety is energetically strongly disfavored (**IV-b**, $\Delta H = +24.4$ kcal mol^{-1} with respect to **I**), consistent with the labeling studies (see Fig. S15).† The hydride in **IV** is expected to be located closer to the second Cr center, leading to two Cr(III) sites. The dimeric bridging Cr(III) hydride species (Fig. 4) are likely EPR silent due to a strong exchange between the neighboring Cr(III) centers. This would contradict the observation of the active Cr(III) sites, as evidenced by CW EPR (Fig. S13).† Therefore, we suggest that the dimeric bridging Cr(III) hydride species (**IV**) split apart to form monomeric Cr(III) sites upon reaction with residual surface OH groups to yield monomeric Cr(III) hydrides **V** and Cr(III) site **V-b**; this process would be energetically favored ($\Delta H = -5.8$ kcal mol^{-1}) as shown in Fig. 4.

All the proposed surface species **I–V** can coordinate CO molecules or allow CO insertion into the Cr–H bond, resulting in characteristic IR bands. We therefore calculated the CO vibrational frequencies (Section S3.2, Fig. S16 & Table S8† for computational details) of all possible Cr species after CO coordination to verify our previous assignments (see Part 1). The DFT calculated IR-CO frequencies obtained from the optimized structures are in good agreement with the assignments discussed above (Section S3.2†).

2.3. Reactivity of Cr(III) hydrides towards ethylene based on calculated reaction pathways

As outlined above, the EP activity of the UC catalyst correlates with the appearance of the dimeric (**IV**) and monomeric (**V**) Cr(III) hydrides (see Part 2), indicating that one of these hydrides could be the active site(s). We then calculated the energy barrier for the activation of ethylene and further chain propagation for sites **IV** and **V** (Fig. S31† and 5, respectively).

Ethylene coordination to the coordinatively unsaturated monomeric Cr(III) hydride **V** and further C_2H_4 insertion into the Cr–H bond is nearly barrier-less ($\Delta H^{\dagger} = 1.1$ kcal mol^{-1}, $\Delta G^{\dagger} = 1.9$ kcal mol^{-1}, Fig. 5). The resulting monomeric Cr(III) alkyl **V-ethyl** ($\Delta H = -16.3$ kcal mol^{-1} for **V-H-C₂H₄**) can undergo chain growth via subsequent C_2H_4 insertions into the Cr–C bond, according to the Cossee–Arlman mechanism.[20,37] This process is
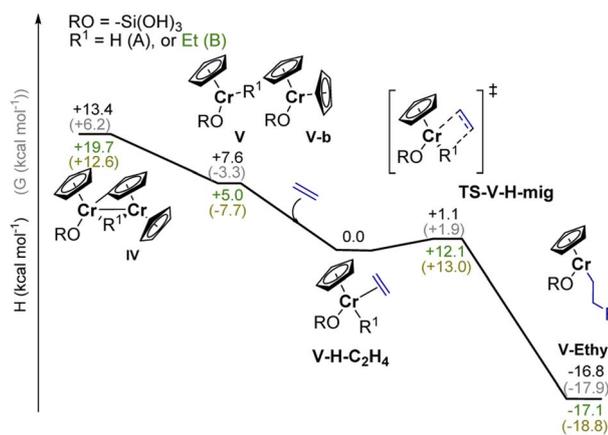
Fig. 5 Calculated reaction enthalpies (H kcal mol^{-1}) and free energies (G kcal mol^{-1}) for potential ethylene activation pathways involving monomeric Cr(III) hydrides such as **V** (in black), or monomeric Cr(III) alkyl species such as **V-ethyl** (in green). Ethylene activation and chain propagation are both associated with reasonable energy costs.

quite similar to what is described for the corresponding reaction of Ti(III) hydrides with C$_2$H$_4$.[20] The obtained **V-ethyl** sites are thus highly active in EP, according to the "augmented" Cossee–Arlman mechanism previously described for the EP-active well-defined Ti(III) alkyls[37] and for heterogeneous Ziegler–Natta catalysts.[38] The subsequent C$_2$H$_4$ insertion has in fact a relatively low calculated TS barrier of $\Delta H = 12.1$ kcal mol^{-1} (Fig. 5). Alternatively, ethylene can coordinate to the Cr atom grafted on the silica surface, while the initially bridging hydride is now localized on the C–H activated chromocene fragment in complex **VI-a** (Fig. S31).† The hydride can migrate to C$_2$H$_4$ while the first Cr–C bond is formed, leading to the formation of a dimeric Cr(III) alkyl complex. However, subsequent chain propagation is energetically prohibited in this case, further supporting that the active sites correspond to monomeric Cr(III) hydrides.

2.4. Synthesis and characterization of well-defined silica-supported Cr(III) alkyl analogs to the UC catalyst

The combination of experimental and computational studies suggest monomeric surface Cr(III) hydrides as the initiating active species. Inspired by the work of Theopold *et al.*,[39,40] we developed CpCr[(CH(SiMe$_3$)$_2$)$_2$] (**4**) (see Fig. 6A) by reacting [CpCrCl$_2$]$_2$ with two equivalents of LiCH(SiMe$_3$)$_2$ (ESI Section 4.1 & Fig. S33† for details on the synthesis and characterization).

Upon contacting **4** with partially dehydroxylated silica (SiO$_2$-$_{700}$), CH$_2$(SiMe$_3$)$_2$ is released. The IR spectrum of **4-SiO$_2$** shows two intense bands at 3126 cm^{-1} and 2955 cm^{-1}, indicating the presence of the [CH(SiMe$_3$)$_2$] ligand (Fig. S3 and S34†), consistent with the formation of surface alkyl species (≡SiO)CrCp[CH(SiMe$_3$)$_2$], whose structure is close to the proposed active sites, **V-ethyl**. Upon exposure to C$_2$H$_4$, **4-SiO$_2$** rapidly polymerize ethylene, as evidenced by the strong C–H bands in the IR spectrum (see Fig. 6B). In fact, the average weight and number molar masses M_w and M_n respectively, as well as the M_w/M_n ratio of the produced PE is essentially the same as the one produced
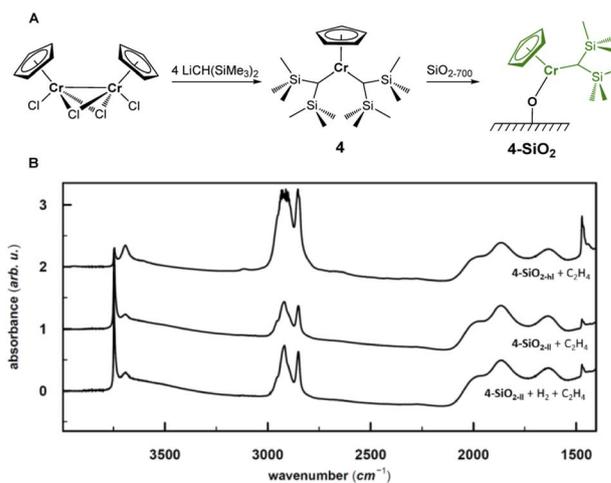

Fig. 6 (A) Synthesis and surface chemistry of **4-SiO$_2$**. (B) IR spectra of **4-SiO$_2$** with high Cr loading (0.8 wt%) after exposure to 25 mbar of C$_2$H$_4$ (top), and **4-SiO$_2$** with low Cr loading (0.2 wt%) after exposure to C$_2$H$_4$ (middle) and H$_2$ (50 mbar) prior to C$_2$H$_4$ (bottom). The higher intensity of C–H bands after exposure of the low Cr-loading material to H$_2$ evidences for slightly higher EP activity.

by the industrial-like UC catalyst (Table S15†), indicating that **4-SiO$_2$** and the UC catalyst contain similar type of active sites.

The CW EPR spectrum[41] of **4-SiO$_2$** (Fig. 7A, black) shows the presence of HS (120–240 mT region) and a LS (300–400 mT region) Cr(III) species. Silica-supported Cr(III) HS species are characterized by a zero-field splitting (ZFS, described by parameters D and E) that exceeds Zeeman interaction at typical magnetic fields and by an effective g tensor ($g_\perp \sim 4$, $g^\parallel \sim 2$), limiting their assignment to structures based on the comparison of g tensor values or exact parameters of the ZFS tensor as the spectra only inform on the ZFS axiality (E/D).[42] The major fraction is represented by a single line in the $g \sim 4$ region, which suggests E/D values close to 0 and is thus indicative of nearly axial symmetry. In contrast, the LS species are best simulated with an orthorhombic g tensor (Fig. S35†). For **4-SiO$_2$**, the axially symmetric HS species can be assigned to the mono-grafted axially symmetric (≡SiO)CrCp[CH(SiMe$_3$)$_2$] surface site, while the LS species likely involve additional interactions of the Cr center with nearby Si–O–Si siloxane bridges. The g tensor principal values for this LS species are close to those obtained for the Cr(III) species of **1-SiO$_2$-1** after its contact with C$_2$H$_4$ (Fig. S36†).

We then focused on pulse EPR investigations of the LS species. As seen from the echo-detected EPR spectrum of **4-SiO$_2$** (Fig. 7A), in pulse EPR spectroscopy at 5 K only the LS component is observable, enabling the selective characterization of these species by 2D hyperfine sublevel correlation (HYSCORE) spectroscopy.[43] These spectra (Fig. 7B and C) reveal the presence of hydrogen atoms magnetically coupled to Cr(III) centers, and weak couplings to ^{29}Si and ^{13}C nuclei. The observation of ^{13}C signals for **4-SiO$_2$** in absence of ^{13}C labeling is indicative of the presence of the Cp ligand within LS Cr(III) species. For ^{1}H, spectral simulation of the observed hyperfine couplings (Fig. 7C) allows to extract the principal values of the ^{1}H hyperfine coupling tensor ($a_{iso} = 3.0$ MHz, $a_{dip} = [-4.75\ -4.75\ 9.5]$ MHz), assuming axial
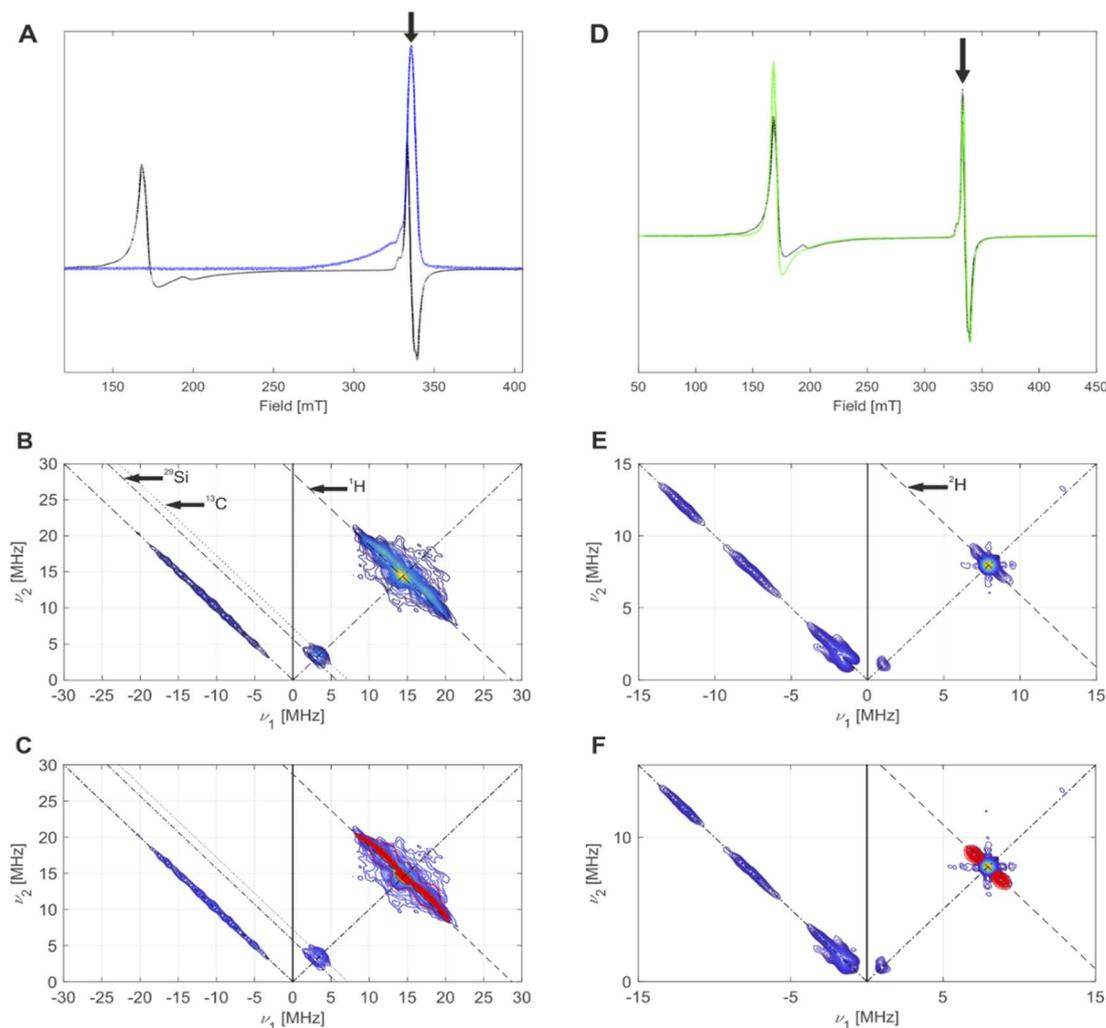
Fig. 7 (A) CW EPR spectrum (black) and echo-detected EPR spectrum (blue) of **4-SiO₂**, measured at 5 K. The black arrow indicates the field position for HYSCORE. (B) HYSCORE spectrum (blue to yellow) of **4-SiO₂**, measured at 5 K. Antidiagonal lines indicate nuclear Zeeman frequencies of magnetically coupled nuclei that are present in this system. (C) Overlay of simulated (red) ^{2}H hyperfine couplings with the experimental HYSCORE spectrum (blue to yellow) from (B) with an overall good agreement to the experimental spectrum. Details on the measurement conditions are outlined in the method Section of the ESI.† (D) CW EPR spectra of **4-SiO₂** before (black) and after (green) EP. The black arrow indicates the field position used for HYSCORE. (E) Q-band HYSCORE spectrum (blue to yellow) of **4-SiO₂** after the C_2D_4 exposure. (F) Overlay of simulated (red) ^{2}H hyperfine couplings with the experimental HYSCORE spectrum (blue to yellow) from (E) with an overall good agreement to the experimental spectrum.

symmetry. Using the point-dipole approximation,[44] we determined a Cr(III)–H distance of 2.55 Å, suggesting α-H atoms of [CH(SiMe₃)₂] ligands in metal-alkyl complexes.[37,45] This allows us to assign the observed $S = 1/2$ ($g = [1.9916; 2.0028; 2.0157]$) species to (≡SiO)CrCp[CH(SiMe₃)₂] surface sites. Note the similar g tensor principal values to **1-SiO₂-1** in presence of C_2H_4 (see Part 1), indicating that similar (≡SiO)CrCp–R species ($R = -(CH_2)_n-CH_3$) are formed in the UC system during EP.

We further performed EPR studies of **4-SiO₂** after its contact with C_2D_4 and observed unchanged principal g tensor values of the investigated LS species (Fig. 7D). In its Q-band HYSCORE spectrum ^{2}H hyperfine couplings (Fig. 7E), with $a_{iso} = 1.7$ MHz, $a_{dip} = [-0.6-0.6\ 1.2]$ MHz and unresolved quadrupole coupling appear (Fig. 7F), indicating that ^{2}H nuclei are in close proximity to the Cr(III) center, consistent with the C_2D_4 insertion into the

Cr(III)–C bond according to the Cossee–Arlman mechanism.[20,37] This is further confirmed by the disappearance of ^{1}H hyperfine couplings in the X-band HYSCORE spectrum of **4-SiO₂** after the C_2D_4 polymerization (Fig. S36†), consistent with its insertion into the Cr(III)–CH(SiMe₃)₂ bond of **4-SiO₂**. Therefore, we propose that the same Cossee–Arlman mechanism is involved in EP on both **4-SiO₂** and the UC catalysts.

3 Conclusions

In this work, we characterized surface sites of the UC silica-supported Cr-based ethylene polymerization catalyst, using SOMC in combination with IR and EPR spectroscopic investigations, labeling experiments, and computational studies. We identified various surface sites depending on the Cr loading.

Monomeric Cr(II) species are formed at very low Cr loading and show no polymerization activity. An increasing Cr loading leads to the formation of dimeric Cr(II) surface sites with various Cr–Cr interactions, that are inactive towards EP. At higher loadings, monomeric Cr(III) hydrides (≡SiO)CrCp–H are formed, their presence correlates with EP activity, and are thus proposed to be the active sites of the UC catalyst. These species are formed via C–H activation at the Cp ring and involvement of surface hydroxyl groups. The presence of a small fraction of adjacent surface OH groups is proposed to be involved in splitting the dimeric Cr(III) hydrides into the monomeric species, which are able to insert ethylene, thus corresponding to the active sites of the UC catalysts. Such structures inspired the preparation of an analog well-defined silica-supported system, namely (≡SiO)CrCp[CH(SiMe$_3$)$_2$] (**4-SiO$_2$**). This material displays similar EPR signatures and EP activity as the UC catalysts and produces polymers of similar molecular weight distribution. Using hyperfine EPR spectroscopy, we also show that the well-defined Cr(III) surface alkyls perform ethylene polymerization via insertion into the Cr(III)–C bond, thus supporting the analog proposition for the EP mechanism for the active species of the UC catalysts. These findings open ways to rationally design novel heterogeneous EP catalysts.

Data availability

All data are provided in the ESI† and additional data can be available upon request.

Conflicts of interest

There are no conflicts to declare.

Acknowledgements

Notes and references

1 M. P. McDaniel, in *Advances in Catalysis*, B. C. Gates and H. Knözinger, eds., Academic Press, 2010, vol 53, pp. 123–606.

2 H. R. Sailors and J. P. Hogan, *J. Macromol. Sci., Part A*, 1981, **15**, 1377–1402.

3 US Pat. 3,709,853, 1973.

4 F. J. Karol, G. L. Karapinka, C. Wu, A. W. Dow, R. N. Johnson and W. L. Carrick, *J. Polym. Sci., Part A: Polym. Chem.*, 1972, **10**, 2621–2637.

5 C. Copéret, F. Allouche, K. W. Chan, M. P. Conley, M. F. Delley, A. Fedorov, I. B. Moroz, V. Mougel, M. Pucino, K. Searles, K. Yamamoto and P. A. Zhizhko, *Angew. Chem., Int. Ed.*, 2018, **57**, 6398–6440.

6 C. Copéret, A. Comas-Vives, M. P. Conley, D. P. Estes, A. Fedorov, V. Mougel, H. Nagae, F. Núñez-Zarur and P. A. Zhizhko, *Chem. Rev.*, 2016, **116**, 323–421.

7 A. Zecchina, G. Spoto and S. Bordiga, *Faraday Discuss. Chem. Soc.*, 1989, **87**, 149–160.

8 M. Schnellbach, F. H. Köhler and J. Blümel, *J. Organomet. Chem.*, 1996, **520**, 227–230.

9 S. L. Fu and J. H. Lunsford, *Langmuir*, 1990, **6**, 1774–1783.

10 F. J. Karol and C. Wu, *J. Polym. Sci., Part A: Polym. Chem.*, 1974, **12**, 1549–1558.

11 F. J. Karol, C. Wu, W. T. Reichle and N. J. Maraschin, *J. Catal.*, 1979, **60**, 68–76.

12 S. L. Fu and J. H. Lunsford, *Langmuir*, 1990, **6**, 1784–1792.

13 K. H. Theopold, R. A. Heintz, S. K. Noh and B. J. Thomas, in *Homogeneous Transition Metal Catalyzed Reactions*, American Chemical Society, 1992, vol 230, ch. 41, pp. 591–602.

14 P. J. Ellis, R. W. Joyner, T. Maschmeyer, A. F. Masters, D. A. Niles and A. K. Smith, *J. Mol. Catal. A: Chem.*, 1996, **111**, 297–305.

15 K. H. Theopold, *Eur. J. Inorg. Chem.*, 1998, **1998**, 15–24.

16 A further increase in the Cr loading on silica (2 wt% Cr, **1-SiO$_2$-2**) does not lead to the appearance of new CO adsorption bands, though the peak at 1579 cm^{-1} gains in intensity.

17 This was previously suggested and confirmed by carrying out the experiment with a 1/1 mixture of ^{12}CO/^{13}CO (see Fig. S5†) and is in agreement with previous assignment, see ref. 6.

18 P. Leoni, A. Landi and M. Pasquali, *J. Organomet. Chem.*, 1987, **321**, 365–369.

19 P. T. Wolczanski and J. E. Bercaw, *Acc. Chem. Res.*, 1980, **13**, 121–127.

20 C. P. Gordon, S. Shirase, K. Yamamoto, R. A. Andersen, O. Eisenstein and C. Copéret, *Proc. Natl. Acad. Sci. U. S. A.*, 2018, **115**, E5867–E5876.

21 M. Pollard, K. Klimke, R. Graf, H. W. Spiess, M. Wilhelm, O. Sperber, C. Piel and W. Kaminsky, *Macromolecules*, 2004, **37**, 813–825.

22 R. Kitamaru, F. Horii and K. Murayama, *Macromolecules*, 1986, **19**, 636–643.

23 R. Blom, I. M. Dahl, A. Follestad and K. J. Jens, *J. Mol. Catal. A: Chem.*, 1999, **138**, 97–102.

24 S. Krimm, C. Y. Liang and G. B. B. M. Sutherland, *J. Chem. Phys.*, 1956, **25**, 549–562.

25 We also observed a weak band at 2887 cm^{-1}, which implies the presence of C–H vibrations, and might be assigned to the end –CD$_2$H group. This is further supported by the presence of two different types of –CD$_2$– symmetric and antisymmetric stretching modes (see Fig. S12A†), indicating the existence of two different types of –CD$_2$– moieties in the produced PE.

26 S. Peitz, N. Peulecke, B. H. Müller, A. Spannenberg and U. Rosenthal, *Acta Crystallogr., Sect. E:*, 2010, **66**, m296–m297.

27 K. A. Kreisel, G. P. A. Yap and K. H. Theopold, *Eur. J. Inorg. Chem.*, 2012, **2012**, 520–529.

28 L. A. MacAdams, G. P. Buffone, C. D. Incarvito, J. A. Golen, A. L. Rheingold and K. H. Theopold, *Chem. Commun.*, 2003, 1164–1165, DOI: 10.1039/B301943H.

29 W. H. Monillas, G. P. A. Yap and K. H. Theopold, *Angew. Chem., Int. Ed.*, 2007, **46**, 6692–6694.

30 J. ashkin, M. L. H. Green, M. L. Poveda and K. Prout, *J. Chem. Soc., Dalton Trans.*, 1982, 2485–2494, DOI: 10.1039/DT9820002485.

31 A. C. Filippou, S. Schneider and G. Schnakenburg, *Angew. Chem., Int. Ed.*, 2003, **42**, 4486–4489.

32 P.-J. Sinnema, P. J. Shapiro, D. M. J. Foo and B. Twamley, *J. Am. Chem. Soc.*, 2002, **124**, 10996–10997.

33 C. J. Harlan, T. Hascall, E. Fujita and J. R. Norton, *J. Am. Chem. Soc.*, 1999, **121**, 7274–7275.

34 R. Choukroun, C. Lorber and B. Donnadieu, *Organometallics*, 2004, **23**, 1434–1437.

35 In contrast, the material 1_{hl-d}-SiO_2-1, shows –CH_2D ending groups after polymerization of C_2H_4, indicating the formation of Cr–D bonds in case of the presence of chemisorbed 1_{d10}.

36 Metalloproteins: Methods and Protocols, ed. J. C. Fontecilla-Camps and N. Yvain, Humana Press, Springer, 2014.

37 A. Ashuiev, F. Allouche, N. Wili, K. Searles, D. Klose, C. Copéret and G. Jeschke, *Chem. Sci.*, 2021, **12**, 780–792.

38 M. F. Delley, F. Núñez-Zarur, M. P. Conley, A. Comas-Vives, G. Siddiqi, S. Norsic, V. Monteil, O. V. Safonova and C. Copéret, *Proc. Natl. Acad. Sci. U. S. A.*, 2014, **111**, 11624–11629.

39 R. A. Heintz, S. Leelasubcharoen, L. M. Liable-Sands, A. L. Rheingold and K. H. Theopold, *Organometallics*, 1998, **17**, 5477–5485.

40 P. A. White, J. Calabrese and K. H. Theopold, *Organometallics*, 1996, **15**, 5473–5475.

41 While both low-spin and high-spin Cr species are observable by CW EPR (see Fig. S13† as an example), pulse EPR investigations of Cr high-spin ($S > 1/2$) species, where zero-field splitting (ZFS) is often the dominant magnetic interaction, is often limited due to short T2 relaxation times, even at temperatures of around 2–20 K (see(*a*) S. Chabbra, D. M. Smith and B. E. Bode, Isolation of EPR spectra and estimation of spin-states in two-component mixtures of paramagnets, *Dalton Trans.*, 2018, **47**, 10473–10479; (*b*) N. A. Hirscher, C. H. Arnett, P. H. Oyala and T. Agapie, Characterization of Cr-Hydrocarbyl Species *via* Pulse EPR in the Study of Ethylene Tetramerization Catalysis, *Organometallics*, 2020, **39**(24), 4420–4429). On the other hand, both high-spin (HS, $S = 3/2$) and low-spin (LS, $S = 1/2$) states were previously observed for Cr(III) alkyl complexes, depending on their ligand surrounding (ref. 29). Also, grafting of the $Cr(N(SiMe_3)_2)_3$ complex on silica, followed by thermal treatment at 400 °C, provided Cr(III) species that are in a LS state, so that pulse EPR measurements were possible already at 110 K (ref. 30).

42 J. Telser, *eMagRes*, 2017, 207–234.

43 P. Höfer, A. Grupp, H. Nebenführ and M. Mehring, *Chem. Phys. Lett.*, 1986, **132**, 279–282.

44 D. M. Murphy, *Proc. Natl. Acad. Sci. U. S. A.*, 2004, **79**, 103.

45 F. Allouche, D. Klose, C. P. Gordon, A. Ashuiev, M. Wörle, V. Kalendra, V. Mougel, C. Copéret and G. Jeschke, *Angew. Chem., Int. Ed.*, 2018, **57**, 14533–14537.